https://doi.org/10.15407/ujpe65.10.904

V.O. ZAMORSKYI,[1] YA.M. LYTVYNENKO,[1] A.M. POGORILY,[1]
A.I. TOVSTOLYTKIN,[1,2] S.O. SOLOPAN,[3] A.G. BELOUS[3]

[1] Institute of Magnetism,
Nat. Acad. of Sci. of Ukraine and Ministry of Education and Science of Ukraine
(36b, Academician Vernadsky Blvd., Kyiv 03142, Ukraine; e-mail: 0vl0ad0@gmail.com)
[2] Taras Shevchenko National University of Kyiv,
Faculty of Radiophysics, Electronics, and Computer Systems
(4g, Academician Glushkov Ave., Kyiv 03127, Ukraine)
[3] V.I. Vernadskyi Institute of General and Inorganic Chemistry, Nat. Acad. of Sci. of Ukraine
(32/34, Academician Palladin Ave., Kyiv 03142, Ukraine)

MAGNETIC PROPERTIES OF $Fe_3O_4/CoFe_2O_4$ COMPOSITE NANOPARTICLES WITH CORE/SHELL ARCHITECTURE

Magnetic properties of the sets of Fe_3O_4(core)/$CoFe_2O_4$(shell) composite nanoparticles with a core diameter of about 6.3 nm and various shell thicknesses (0, 1.0, and 2.5 nm), as well as the mixtures of Fe_3O_4 and $CoFe_2O_4$ nanoparticles taken in the ratios corresponding to the core/shell material contents in the former case, have been studied. The results of magnetic research showed that the coating of magnetic nanoparticles with a shell gives rise to the appearance of two simultaneous effects: the modification of the core/shell interface parameters and the parameter change in both the nanoparticle's core and shell themselves. As a result, the core/shell particles acquire new characteristics that are inherent neither to Fe_3O_4 nor to $CoFe_2O_4$. The obtained results open the way to the optimization and adaptation of the parameters of the core/shell spinel-ferrite-based nanoparticles for their application in various technological and biomedical domains.

Keywords: nanoparticles, core/shell architecture, core, shell, magnetization, blocking temperature.

1. Introduction

The core/shell architecture of nanoparticles attracts considerable interest, because it allows materials with different properties to be combined and nanostructures with controlled magnetic characteristics to be manufactured. In addition to variations in the size, shape, and composition of specimens, the control over the material properties by combining different magnetic materials and making a purposeful impact on the near-interface region becomes a dominant trend, in which a new factor for the development of materials with improved characteristics is introduced. Recent studies have demonstrated the advantages of the core/shell architecture, when enhancing the efficiency of dc magnets, increasing the heat resistance of magnetic nanocrystals in order to overcome the "superparamagnetic limit" for information media, and optimizing the parameters of nanoparticles in biomedical applications [1–5]. The study of core/shell combinations of different magnetic materials broadens our body of knowledge concerning magnetic interactions at the nanoscale level and creates conditions for achieving the desired magnetic parameters in various applications.

The ferrite spinel system $M\mathrm{Fe_2O_4}$ (M = Fe, Co, Mn, and so forth) is one of the most important and widely used magnetic materials. It includes both magnetically hard and magnetically soft materials. For example, cobalt ferrite $CoFe_2O_4$ is a magnetically hard material with the magnetocrystalline anisotropy constant $K > 10^5$ J/m^3 [3, 5]. On the other hand, magnetite Fe_3O_4 is a ferrite with the much lower magnetic anisotropy constant $K > 10^3 \div 10^4$ J/m^3 [6, 7]. Nevertheless, owing to the identical crystalline

structure and similar crystallographic parameters of those ferrite spinels, the epitaxial growth of a continuous shell made from one of those materials around the nanoparticle core made from the other material becomes possible. Such approach to the production and study of nanoparticles with the core/shell architecture can provide a reliable basis for a thorough explanation and a more profound understanding of magnetism in nanostructured materials, as well as the relations connecting their crystalline structures, morphology, and physical properties.

Currently, there are only a few studies in this direction [3, 8–11]. Issues giving rise to a full understanding of the influence of the core/shell architecture on the magnetization and the effective anisotropy of magnetic nanoparticles, as well as the role of interface effects in the formation of magnetic properties of composite nanostructures of this type, still remain open.

In this work, we will compare the magnetic properties of Fe_3O_4(core)/$CoFe_2O_4$(shell) nanoparticles with the properties of the mixtures of Fe_3O_4 and $CoFe_2O_4$ nanoparticles taken in the corresponding ratios. Attention was focused on the role of interface phenomena occurring at the $Fe_3O_4/CoFe_2O_4$ interface in the formation of the magnetic properties of core/shell nanoparticles. The methods of purposeful control over the magnetic parameters of composite nanostructures were discussed from the viewpoint of various technological and biomedical applications.

2. Experimental Specimens and Procedure

The synthesis of nanostructures with the core/shell architecture is a rather complicated procedure, because it must provide a high crystallinity degree in both the core and the shell, guarantee a high-quality epitaxy, and minimize the mixing processes at the core/shell interface. That is why when producing $Fe_3O_4/CoFe_2O_4$ composite nanoparticles, we account for the results of previous works performed by our and other research groups [9–13]. In our previous works, the combined application of X-ray diffraction and Mössbauer spectroscopy to ^{57}Fe nuclei allowed us to draw conclusion that, among the methods used to synthesize magnetic nanoparticles (MNPs), the method of co-precipitation from a diethylene glycol (DEG) solution makes it possible to fabricate magnetite nanoparticles with the least amount of the maghemite and goethite phases [10, 12]. Therefore, this method was used in the present work as well.

While synthesizing Fe_3O_4 and $CoFe_2O_4$ nanoparticles, as well as $Fe_3O_4/CoFe_2O_4$ composite MNPs, the following initial reagents were applied: iron (III) chloride nonahydrate (97% $FeCl_3 \cdot 9H_2O$, Sigma Aldrich), cobalt (II) nitrate hexahydrate (98% $Co(NO_3)_2 \cdot 6H_2O$, Sigma Aldrich), iron (II) sulfate heptahydrate (99% $FeSO_4 \cdot 7H_2O$, Sigma Aldrich), sodium hydroxide (98% NaOH), and diethylene glycol (99% DEG, Sigma Aldrich).

For the synthesis of Fe_3O_4 and $CoFe_2O_4$ nanoparticles, the initial reagents were taken in a stoichiometric ratio of 2 : 1 ($Fe^{3+} : Fe^{2+}$ or $Fe^{3+} : Co^{2+}$). Then they were mixed with diethylene glycol, and the solution was stirred for 1 h. Simultaneously, the solution of NaOH in DEG was prepared. The alkaline solution was added dropwise to the former solution, and the mixture was stirred again for 1 h. The obtained reaction mixture was heated up to a temperature of 200°C at a rate of 2–3°C/min and kept at this temperature for 1.5 h. The synthesis allowed us to fabricate Fe_3O_4 and $CoFe_2O_4$ magnetic nanoparticles with average sizes of about 6.3 and 4.1 nm, respectively, [8]. The synthesized Fe_3O_4 and $CoFe_2O_4$ nanoparticles in the form of their solutions in diethylene glycol were used to prepare mixtures of Fe_3O_4 and $CoFe_2O_4$ nanoparticles with the mass ratios between the components corresponding to the mass ratios between the core and shell materials in each core/shell specimen.

On the other hand, for the synthesis of $Fe_3O_4/CoFe_2O_4$ composite nanoparticles, a solution for the creation of the $CoFe_2O_4$ shell was prepared at the first stage. Namely, $Co(NO_3)_2 \cdot 6H_2O$ and $FeCl_3 \cdot 9H_2O$, which were taken in a molar ratio of 1 : 2, were dissolved in DEG, and the solution was stirred for 1 h. Simultaneously, the solution of NaOH in DEG was prepared. The alkaline solution was added dropwise to the solution of the salt mixture $Co(NO_3)_2 \cdot 6H_2O$ and $FeCl_3 \cdot 9H_2O$, and the obtained mixture was stirred again for 1 h. Afterward, the solution with the previously synthesized core nanoparticles (Fe_3O_4) was added to the resulting reaction mixture, and the resulting product was stirred again for 1 h under the ultrasound action. The obtained reaction mixture was heated up to a temperature of 200 °C at a rate of 2–3 °C/min and kept at this temperature for 1.5 h. Then oleic acid was added, and the mixture was stirred for 10 min. The resulting precipitate was

cooled down and centrifuged. Then it was dispersed once more in ethanol and dried in air at a temperature of 30 °C.

The amount of $CoFe_2O_4$ needed to synthesize a shell with a required thickness was determined according to the following algorithm. The volume of the material required for the shell of one core/shell particle, V_{shell}, was calculated according to the formula $V_{\text{shell}} = \frac{4}{3}\pi\left(R_2^3 - R_1^3\right)$, where R_1 and R_2 are the radii of the uncoated and coated, respectively, particles. The mass of the shell material per one particle, m_{shell}, was found as $m_{\text{shell}} = \rho V_{\text{shell}}$, where ρ is the shell material density. The mass of the core material per particle, m_{core}, was calculated in the same way. The known value of the ratio $m_{\text{shell}}/m_{\text{core}}$ made it possible to determine the mass of the shell material for any selected mass of the core material. For instance, in order to coat 1 g of Fe_3O_4 nanoparticles possessing an average core size of 6.3 nm with a shell 1 nm in thickness, 1.287 g of $CoFe_2O_4$ is required.

According to the method described above, Fe_3O_4/$CoFe_2O_4$ composite MNPs with a fixed core diameter of about 6.3 nm and effective shell thicknesses of 0, 1.0, and 2.5 nm (hereafter, specimens S0, S1, and S2, respectively) were synthesized. We also prepared mixtures of Fe_3O_4 and $CoFe_2O_4$ nanoparticles with mass ratios of 1 : 1.2 and 1 : 5 (hereafter, specimens Mix1 and Mix2, respectively), which corresponded to the shell/core mass ratios for the nanoparticles in specimens S1 and S2, respectively.

The synthesized materials were studied on an X'Pert PANalytical diffractometer (at a 45 kV voltage and a 40 mA current using Ni filtered Co-$K\alpha$ radiation) with the help of the X-ray diffraction method. The radiation intensity distribution and the X-ray peak angles for both pure initial compounds and core/shell nanoparticles were calculated using the PeakFit 4.12 software by analyzing separate experimental peaks with maximum intensities in the interval of 2θ-angles from 38° to 46°. The exposure duration was 30 s per experimental point. The size and morphology of the researched nanoparticles were determined with the help of a scanning electron microscope JEM-1230.

Magnetic measurements were performed in a temperature interval of 5–400 K using a commercial device Quantum Design Physical Property Measurement System, which was equipped with a vibration magnetometer. The magnetic moment was measured when heating the specimen in the field $H_{\text{measur}} = 50$ Oe after its cooling in the zero magnetic field (the ZFC mode). The isothermal hysteresis loops were measured at temperatures of 5 and 300 K in magnetic fields up to 90 kOe.

3. Research Results

The results of X-ray diffraction studies of the synthesized nanostructures were analyzed in work [8] in detail. All synthesized specimens had a cubic spinel structure (ICDD 19-0629) and were absolutely free of any impurity phases.

According to the results of electron microscopy research, the average size of Fe_3O_4 magnetic nanoparticles was about 6.3 nm [8]. As the effective thickness of the $CoFe_2O_4$ shell increased, the average particle size also increased in accordance with the results of preliminary calculations.

Figure 1 demonstrates the magnetic hysteresis loops for all researched specimens (these are specimens S0, S1, S2, Mix1, and Mix2) measured at a temperature of 5 K. In both specimen series, the growth of the $CoFe_2O_4$ content strongly affects the loop shape by modifying its parameters, in particular, the saturation magnetization M_s and the coercive force H_c.

For the Fe_3O_4 and $CoFe_2O_4$ nanoparticles, the saturation magnetization amounted to 77 and 50 A m^2/kg, respectively, at the temperature $T = 5$ K. It is worth noting that the corresponding values of M_s for the bulk specimens equaled 98 and 94 A m^2/kg, respectively, [15]. The reduced magnetization of nanoparticles can be a result of the appreciable contribution from near-surface layers, which are characterized, as a rule, by a larger magnetic disorder [8]. A conclusion can also be drawn that the contribution of near-surface layers to the nanoparticle magnetization is larger in the $CoFe_2O_4$ magnetic nanoparticles than in the Fe_3O_4 ones.

The creation of a shell around the core and its further growth led to a substantial transformation of the loop shape. In particular, the values of both the saturation magnetization M_s and the coercive force H_c changed. The initial coating of MNPs ($t_{\text{shell}} = 1.0$ nm) did not considerably affect the M_s value. But the growth of the shell thickness to 2.5 nm resulted in a reduction of the M_s value to 64 A m^2/kg. Such behavior may be associated with an enhanced contribution of the $CoFe_2O_4$ shell, which

demonstrated a reduced magnetization in the nanoscale regime [8, 16, 17].

A drastic increase of the H_c value from about 370 Oe to about 6.8 kOe (i.e., by more than an order of magnitude) was observed for the initial MNP coating with the thickness $t_{shell} = 1.0$ nm. As the shell thickness increased, the coercive force also increased and reached a value of about 10.1 kOe for specimen S2 with $t_{shell} = 2.5$ nm. Those effects can be explained, if we assume a simultaneous action of two factors: (i) the modification of the parameters characterizing the phase interface between the core and the shell and (ii) the contribution of the magnetically hard shell to the growth of the total coercivity. Since the coercivity of single-domain MNPs is coupled with the effective anisotropy constant K_{eff} [18], the data exhibited in Fig. 1 make it possible to draw a preliminary conclusion that the emergence of the shell and the subsequent growth of its thickness are responsible for the strong increase of K_{eff}. It is worth noting that a similar behavior was observed for the core/shell $MnFe_2O_4/CoFe_2O_4$ and $ZnFe_2O_4/CoFe_2O_4$ nanoparticles [3, 19, 20].

The character of the M_s and H_c variation in Mix1 and Mix2 specimens was close to that observed in S1 and S2 specimens. Namely, an increase of the $CoFe_2O_4$ content led to a saturation magnetization reduction and a coercive force growth, but the magnitudes of the M_s and H_c changes in Mix1 and Mix2 specimens were less pronounced. The distorted shape of the hysteresis loops for those specimens may arise because the particles could rotate in the course of the remagnetization process [21].

In Fig. 2, the temperature dependences of the magnetization of researched specimens, $M_{ZFC}(T)$, are shown. To register the dependence $M_{ZFC}(T)$, the specimen was cooled down from room temperature to 5 K in the zero magnetic field. Then the external magnetic field $H_{measur} = 50$ Oe was applied to the specimen, and the parameter M_{ZFC} was measured as a function of the temperature during the process of specimen heating. One can see that each $M_{ZFC}(T)$ dependence in Fig. 2 has a maximum at a certain temperature T_b, which is called the blocking temperature. The appearance of the maximum in the $M_{ZFC}(T)$ dependence testifies that, near T_b, the anisotropy energy of nanoparticles, $K_{eff}V$, becomes comparable with the thermal energy kT (here, V is the particle volume, and k the Boltzmann constant). At the temperatures $T < T_b$, the magnetic moments of most nanoparticles are blocked, and their orientation is determined by the anisotropy energy (field). At the temperatures higher than the blocking temperature, the behavior of most nanoparticles is superparamagnetic [8].

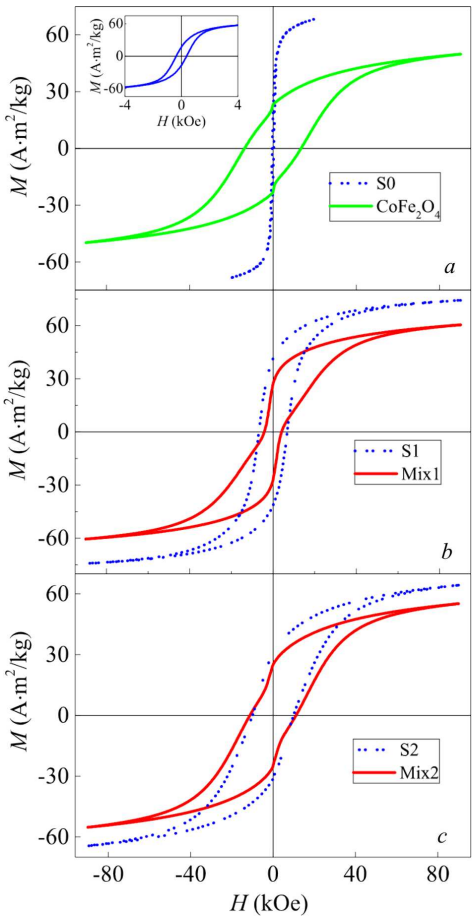

Fig. 1. Dependences of specimen magnetization on the magnetic field strength. The measurements were made at the temperature $T = 5$ K. The inset in panel (a) demonstrates the dependence $M(H)$ for specimen S0 at low magnetic fields

Specimen S1 has a single blocking temperature. It means that the spins in the nanoparticle core and shell are strongly bound and jointly respond to the temperature and magnetic field changes. For the MNPs with a shell thickness of 2.5 nm (specimen S2), two peaks are observed. They can be generated by separate contributions from the nanoparticle core and the nanoparticle shell because the thickness of the latter is rather substantial.

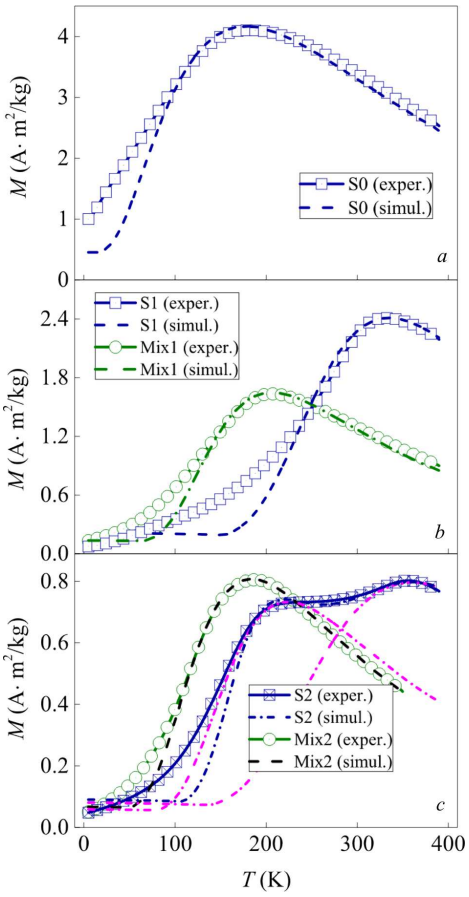

Fig. 2. Dependences $M_{\mathrm{ZFC}}(T)$ for researched specimens registered in the magnetic field $H_{\mathrm{measur}} = 50$ Oe. The dashed curves correspond to calculated dependences obtained using formula (1). See further explanations in the text

For specimens S0, S1, and S2, the T_{b} value increases from about 175 K (without the coating) to about 328 K (with the initial MNP coating by the $CoFe_2O_4$ shell with $t_{\mathrm{shell}} = 1.0$ nm) and reaches about 356 K for the specimen with $t_{\mathrm{shell}} = 2.5$ nm. Such behavior is in agreement with the conclusion made above about the increase of the effective anisotropy constant K_{eff}, which is associated with the creation of the shell and the subsequent increase of its thickness. Further-more, the increase of the total volume of MNPs also contributes to this trend, because the T_{b} value is related to the product $K_{\mathrm{eff}}V$ [22, 23]. It should be noted that the blocking temperature in specimens Mix1 and Mix2 remains almost the same as in the initial specimen S0, although the average size of nanoparticles decreases.

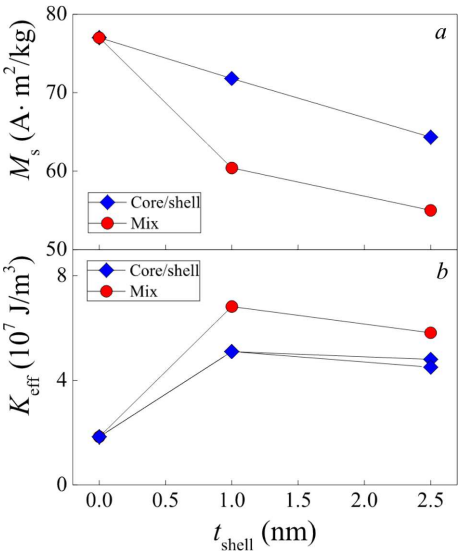

Fig. 3. Dependences of the saturation magnetization M_{s} (a) and the effective anisotropy constant K_{eff} (b) on the $CoFe_2O_4$ content in the studied specimens

For a deeper understanding of the processes that govern the behavior of examined specimens, a more detailed analysis of the obtained data was made. A simple model of noninteracting single-domain particles was used to describe the experimental dependences $M_{\mathrm{ZFC}}(T)$ that are shown in Fig. 2. At every temperature, the ensemble of nanoparticles can be divided into two groups depending on their size. These are nanoparticles dwelling in an ideal superparamagnetic state (their volume V is below a certain critical value V_{c}) and nanoparticles the magnetic moments of which remain blocked (their volume $V > V_{\mathrm{c}}$). As a result, we obtain

$$\frac{M_{\mathrm{ZFC}}}{M_s} = \left[\int_0^{V_c} L(M_s HV/kT)V\, f(V)dV + \right.$$
$$\left. + \int_{V_c}^{\infty} (M_s H/3K_{\mathrm{eff}})V\, f(V)dV\right] V\, f(V)dV, \qquad (1)$$

where $L(x)$ is the Langevin function, and $f(V)$ the distribution function of nanoparticles over their volumes. The first term in the numerator is written in the approximation that the energy barrier, which is defined as the product $K_{\mathrm{eff}}V$, is much lower than the thermal energy kT, so that such a barrier can be neglected. In this case, the response of the magnetiza-

tion to a magnetic field or temperature (H or T) variation is described by the Langevin function. The second term is a result of the initial susceptibility of randomly oriented, blocked, single-domain nanoparticles with the effective anisotropy coefficient K_{eff}. The boundary between the two groups is determined by the critical volume

$$V_{\text{c}} = \frac{kT}{K_{\text{eff}}} \ln\left(\frac{\tau_{\text{m}}}{\tau_0}\right), \tag{2}$$

where τ_m is a characteristic measurement time, and $\tau_0 = 10^{-9}$ s [10, 25]. For quasistatic measurements, the parameter τ_m was chosen to equal 100 s.

The calculation results are shown in Fig. 2 by dashed curves. In the course of calculations, the MNP volume distribution was approximated by the log-normal function, which was chosen according to the transmission electron microscopy data [8]. The electron microscopy data were also used to determine the average size of nanoparticles in each specimen (this parameter was considered to be a fixed one). In order to obtain the maximum agreement between the experimental and calculated data, the width of the volume distribution function and the K_{eff} value were varied. The approximation results were used to obtain the K_{eff} values for all studied specimens.

Figure 3 illustrates the dependences of the effective anisotropy constant K_{eff} and the saturation magnetization M_{s} on the shell thickness t_{s} for the examined specimens. One can see that the growth of the $CoFe_2O_4$ content leads to the growth of the effective anisotropy constant and the reduction of the saturation magnetization. Those changes are less pronounced for specimens S1 and S2 as compared with those for specimens Mix1 and Mix2. It is evident that the creation of the $CoFe_2O_4$ shell around a Fe_3O_4 nanoparticle changes the parameters of both the initial nanoparticle and the shell around it. As a result, the core/shell nanoparticles acquire new characteristics, which are not inherent to both the core (Fe_3O_4) and the shell ($CoFe_2O_4$) materials.

The results concerning the regularities in the dependences of the core/shell nanoparticle properties on the shell thickness t_{shell}, which were obtained in this work and in works [8, 26], open the way to a purposeful control over the magnetic parameters of composite nanostructures in various technological and biomedical applications.

4. Conclusions

The magnetic properties of composite nanoparticles with the core/shell architecture were studied. The nanoparticle core (Fe_3O_4) had a fixed diameter of about 6.3 nm, whereas the effective shell ($CoFe_2O_4$) thickness was varied: $t_{\text{shell}} = 0$, 1.0, and 2.5 nm. The magnetic characteristics for the ensembles of those nanoparticles were determined and compared with their counterparts for the mixtures of Fe_3O_4 and $CoFe_2O_4$ nanoparticles taken in the corresponding ratios.

On the basis of the results of magnetometric studies, it was shown that the shell thickness in the $Fe_3O_4/CoFe_2O_4$ composite magnetic nanoparticles strongly affects the hysteresis loop shape and the temperature dependence of the magnetization. In the framework of a simple model for coexisting superparamagnetic and blocked magnetic nanoparticles, the effective anisotropy constants were calculated. A conclusion was drawn that the creation of a $CoFe_2O_4$ shell around a Fe_3O_4 nanoparticle leads to the parameter change in both the initial nanoparticle and its shell. As a result, nanoparticles with the core/shell architecture acquire new characteristics, which are inherent neither to the core (Fe_3O_4) nor to the shell ($CoFe_2O_4$) material.

The obtained results open the way to the optimization and adaptation of the parameters of the core/shell nanoparticles fabricated on the basis of ferrite spinels and intended for application in various technological and biomedical domains.

The work was partially sponsored by the Ministry of Education and Science of Ukraine (project No. 0118U003790) and the National Academy of Sciences of Ukraine (project No. 0119U100469), as well as by the target research program of the National Academy of Sciences of Ukraine "Materials for medicine and medical equipment" (project No. 4.4/20).

1. P. Mélinon, S. Begin-Colin, J.L. Duvail, F. Gauffre, N.H. Boime, G. Ledoux, J. Plain, P. Reiss, F. Silly, B. Warot-Fonrose. Engineered inorganic core/shell nanoparticles. *Phys. Rep.* **543**, 163 (2014).
2. S.H. Noh, W. Na, J.T. Jang, J.H. Lee, E.J. Lee, S.H. Moon, Y. Lim, J.S. Shin, J. Cheon. Nanoscale magnetism control via surface and exchange anisotropy for optimized ferrimagnetic hysteresis. *Nano Lett.* **12**, 3716 (2012).

3. Q. Song, Z.J. Zhang. Controlled synthesis and magnetic properties of bimagnetic spinel ferrite $CoFe_2O_4$ and $MnFe_2O_4$ nanocrystals with core-shell architecture. *J. Am. Chem. Soc.* **134**, 10182 (2012).
4. J.H. Lee, J.T. Jang, J.S. Choi, S.H. Moon, S.H. Noh, J.W. Kim, J.G. Kim, I.S. Kim, K.I. Park, J. Cheon. Exchange-coupled magnetic nanoparticles for efficient heat induction. *Nature Nanotech.* **6**, 418 (2011).
5. A.A. Sattar, H.M. El-Sayed, I. Alsuqia. Structural and magnetic properties of $CoFe_2O_4/NiFe_2O_4$ core/shell nanocomposite prepared by the hydrothermal method. *J. Magn. Magn. Mater.* **395**, 89 (2015).
6. A.H. Habib, C.L. Ondeck, P. Chaudhary, M.R. Bockstaller, M.E. McHenry. Evaluation of iron-cobalt/ferrite core-shell nanoparticles for cancer thermotherapy. *J. Appl. Phys.* **103**, 07A307 (2008).
7. R. Ghosh, L. Pradhan, Y.P. Devi, S.S. Meena, R. Tewari, A. Kumar, S. Sharma, N.S. Gajbhiye, R.K. Vatsa, B.N. Pandey, R.S. Ningthoujam. Induction heating studies of Fe_3O_4 magnetic nanoparticles capped with oleic acid and polyethylene glycol for hyperthermia. *J. Mater. Chem.* **21**, 13388 (2011).
8. D. Polishchuk, N. Nedelko, S. Solopan, A. Ślawska-Waniewska, V. Zamorskyi, A. Tovstolytkin, A. Belous. Profound interfacial effects in $CoFe_2O_4/Fe_3O_4$ and $Fe_3O_4/CoFe_2O_4$ core/shell nanoparticles. *Nanoscale Res. Lett.* **13**, 67 (2018).
9. T. Gaudisson, R. Sayed-Hassan, N. Yaacoub, G. Franceschin, S. Nowak, J.M. Grenèche, N. Menguy, P. Sainctavit, S. Ammar. On the exact crystal structure of exchange-biased Fe_3O_4-CoO nanoaggregates produced by seed-mediated growth in polyol. *Cryst. Eng. Commun.* **18**, 3799 (2016).
10. O.V. Yelenich, S.O. Solopan, J.M. Grenèche, A.G. Belous. Synthesis and properties MFe_2O_4 (M = Fe, Co) nanoparticles and core-shell structures. *Solid State Sci.* **46**, 19 (2015).
11. N. Flores-Martinez, G. Franceschin, T. Gaudisson, P. Beaunier, N. Yaacoub, J.-M. Grenèche, R. Valenzuela, S. Ammar. Giant exchange-bias in polyol-made $CoFe_2O_4$-CoO core-shell like nanoparticles. *Part. Part. Syst. Char.* **35**, 1800290 (2018).
12. O.V. Yelenich, S.O. Solopan, T.V. Kolodiazhnyi, J.M. Grenèche, A.G. Belous. Synthesis of iron oxide nanoparticles by different methods and study of their properties. *Solid State Phenom.* **230**, 108 (2015).
13. G. Franceschin, T. Gaudisson, N. Menguy, B.C. Dodrill, N. Yaacoub, J.M. Grenèche, R. Valenzuela, S. Ammar. Exchange-biased $Fe_{3-x}O_4$-CoO granular composites of different morphologies prepared by seed-mediated growth in polyol: From core-shell to multicore embedded structures. *Part. Part. Syst. Char.* **35**, 1800104 (2018).
14. S. Mornet, C. Elissalde, V. Hornebecq, O. Bidault, E. Duguet, A. Brisson, M. Maglione. Controlled growth of silica shell on $Ba_{0.6}Sr_{0.4}TiO_3$ nanoparticles used as precursors of ferroelectric composites. *Chem. Mater.* **17**, 4530 (2005).
15. S. Chikazumi. *Physics of Ferromagnetism* (Oxford Univ. Press, 1997).
16. Y.O. Tykhonenko-Polishchuk, N.N. Kulyk, O.V. Yelenich, V. Bečyte, K. Mažeika, V.M. Kalita, A.G. Belous, A.I. Tovstolytkin. Quasi-static magnetic properties and high-frequency energy losses in $CoFe_2O_4$ nanoparticles. *Low Temp. Phys.* **42**, 470 (2016).
17. N. Daffé, F. Choueikani, S. Neveu, M.A. Arrio, A. Juhin, P. Ohresser, V. Dupuis, P. Sainctavit. Magnetic anisotropies and cationic distribution in $CoFe_2O_4$ nanoparticles prepared by co-precipitation route: Influence of particle size and stoichiometry. *J. Magn. Magn. Mater.* **460**, 243 (2018).
18. J. Carrey, B. Mehdaoui, M. Respaud. Simple models for dynamic hysteresis loop calculations of magnetic single-domain nanoparticles: Application to magnetic hyperthermia optimization. *J. Appl. Phys.* **109**, 083921 (2011).
19. Q. Zhang, I. Castellanos-Rubio, R. Munshi, I. Orue, B. Pelaz, K.I. Gries, W.J. Parak, P. del Pino, A. Pralle. Model driven optimization of magnetic anisotropy of exchange-coupled core-shell ferrite nanoparticles for maximal hysteretic loss. *Chem. Mater.* **27**, 7380 (2015).
20. O. Masala, D. Hoffman, N. Sundaram, K. Page, T. Proffen, G. Lawes, R. Seshadri. Preparation of magnetic spinel ferrite core/shell nanoparticles: Soft ferrites on hard ferrites and vice versa. *Solid State Sci.* **8**, 1015 (2006).
21. V.M. Kalita, D.M. Polishchuk, D.G. Kovalchuk, A.V. Bodnaruk, S.O. Solopan, A.I. Tovstolytkin, S.M. Ryabchenko, A.G. Belous, Interplay between superparamagnetic and blocked behavior in an ensemble of lanthanum-strontium manganite nanoparticles. *Phys. Chem. Chem. Phys.* **19**, 27015 (2017).
22. V.M. Kalita, A.I. Tovstolytkin, S.M. Ryabchenko, O.V. Yelenich, S.O. Solopan, A.G. Belous. Mechanisms of AC losses in magnetic fluids based on substituted manganites. *Phys. Chem. Chem. Phys.* **17**, 18087 (2015).
23. S. Bedanta, A. Barman, W. Kleemann, O. Petracic, T. Seki. Magnetic nanoparticles: A subject for both fundamental research and applications. *J. Nanomater.* **2013**, 952540 (2013).
24. C. Antoniak, M. Farle. Magnetism at the nanoscale: The case of FePt. *Mod. Phys. Lett. B* **21**, 1111 (2007).
25. O. Yelenich, S. Solopan, T. Kolodiazhnyi, Y. Tykhonenko, A. Tovstolytkin, A. Belous. Magnetic properties and ac losses in AFe_2O_4 (A = Mn, Co, Ni, Zn) nanoparticles synthesized from nonaqueous solution. *J. Chem.* **2015**, 532198 (2015).
26. S.O. Solopan, N. Nedelko, S. Lewińska, A. Ślawska-Waniewska, V.O. Zamorskyi, A.I. Tovstolytkin, A.G. Belous. Core/shell architecture as an efficient tool to tune DC magnetic parameters and AC losses in spinel ferrite nanoparticles. *J. Alloys Compd.* **788**, 1203 (2019).

Received 11.07.20.
Translated from Ukrainian by O.I. Voitenko

В.О. Заморський, Я.М. Литвиненко, А.М. Погорілий, О.І. Товстолиткін, С.О. Солопан, А.Г. Білоус

МАГНІТНІ ВЛАСТИВОСТІ
КОМПОЗИТНИХ НАНОЧАСТИНОК $Fe_3O_4/CoFe_2O_4$
З АРХІТЕКТУРОЮ ЯДРО/ОБОЛОНКА

Р е з ю м е

Проведено дослідження магнітних властивостей двох типів наночастинок: наночастинок з архітектурою ядро/оболонка (core/shell) $Fe_3O_4/CoFe_2O_4$ з товщиною ядра ∼6,3 нм і змінною товщиною оболонки (0; 1,0; 2,5 нм) та суміші окремих наночастинок Fe_3O_4 і $CoFe_2O_4$ у співвідношеннях, що відповідають концентраціям компонент наночастинок ядро/оболонка. Аналіз результатів магнітометрії показує, що покриття магнітних наночастинок оболонкою приводить до двох одночасних ефектів: модифікації параметрів міжфазної границі між ядром та оболонкою та трансформації параметрів як вихідної наночастинки, так і її оболонки, в результаті чого core/shell наночастинки набувають нових характеристик, які не характерні ні для ядра (Fe_3O_4), ні для оболонки ($CoFe_2O_4$), ні для механічної суміші на їх основі. Отримані результати відкривають шляхи до оптимізації та адаптації параметрів core/shell наночастинок на основі феритів-шпінелей для їх використання в різних технологічних і біомедичних галузях.